Available online at www.sciencedirect.com
ScienceDirect
Polymer 48 (2007) 6605–6616
polymer
www.elsevier.com/locate/polymer

Multi-month thermal aging of electro-optic polymer waveguides: Synthesis, fabrication, and relaxation modeling

Geoffrey A. Lindsay [a,*], Andrew J. Guenthner [a], Michael E. Wright [a], Mohan Sanghadasa [b], Paul R. Ashley [c]

[a] U.S. Navy, NAVAIR, Chemistry Division, China Lake, CA 93555-6100, USA
[b] The AEgis Technologies Group, Inc., Huntsville, AL 35806, USA
[c] U.S. Army, AMRDEC, RD&E Command, Redstone Arsenal, AL 35898, USA

Received 31 July 2007; received in revised form 18 August 2007; accepted 22 August 2007
Available online 31 August 2007

Abstract

The preparation of polyimides containing side-chain chromophores and the long-term aging performance of poled films are described. These materials were compared to guest–host polycarbonate films. Mach–Zehnder optical interferometers were fabricated from these polymers that contained CLD- and FTC-type chromophores. Changes in optical properties were monitored for months at four temperatures ranging from ambient to 110 °C. The isothermal relaxation data were modeled using both a stretched exponential equation and a power law in time equation. The temperature dependency of the time constants of these equations was modeled using a new activation-energy equation: $\ln(\tau/\tau_p) = E_R(1 + \tanh[(T_c - T)/D])/2RT + E_p/RT$ where T_c is the central temperature of the transition zone, D is the breadth of the zone, and Es are the activation energies of rigid and pliable materials. Multi-year high-temperature stability of the poled guest–host and side-chain materials was predicted.

Keywords: Aging; Chromophore; Nonlinear optic

1. Introduction

Electro-optic (EO) polymers hold great promise for use in optical communicating, sensing and computing systems. Polymer optical waveguide modulators that use less than 1 V to operate ($V_\pi < 1$ V) [1] and their operation at frequencies as high as 165 GHz [2] have been demonstrated. EO polymer films containing the general class of CLD and FTC chromophores that were first reported in the late 1990s [3,4] generated considerable interest because they have a higher EO coefficient (r_{33}) than lithium niobate. Shortly thereafter, work began in our laboratory to synthesize several versions of these second-generation chromophores to incorporate them into polymers by two different methods and to measure their thin-film properties. Initial inspection indicated that these materials had adequate thermal stability to build prototype optical modulators. Recently we reported methods of integrating optical waveguides of these materials on silicon substrates using ''silicon optical bench'' architecture [5].

An amorphous thermoplastic EO polymer modulator, after months of operation at elevated temperatures, can have a noticeable decrease of the EO coefficient (an increase of the operating voltage), which is due to the slow rotational diffusion of the chromophores. We and others have found that EO films with a sufficiently high T_g (>140 °C) exhibit very little decay when stored for years at room temperature. However, when the EO film is heated to the T_g, the polar order completely relaxes within minutes. Measuring and predicting the long-term aging behavior at extreme operating conditions using state-of-the-art EO polymer modulators were the main objectives of this study.

* Corresponding author. Tel.: +1 81 760 939 1630; fax: +1 81 760 939 1617.
E-mail address: geoffrey.lindsay@navy.mil (G.A. Lindsay).

0032-3861/$ - see front matter © 2007 Elsevier Ltd. All rights reserved.
doi:10.1016/j.polymer.2007.08.057

The relaxation rate of poled order in EO films (the rate of decrease in r_{33}) has often been measured by monitoring the decrease in second harmonic generation (SHG) upon irradiating the film with a pulsed laser [6,7]. SHG is a measure of the second-order nonlinear susceptibility, d_{33}, which is directly proportional to the r_{33}. A useful way to directly monitor the EO r_{33} coefficient is the modified Teng–Man method [8], in which an electric field is applied across the film with transparent electrode(s) to modulate a reflected (transmitted) light beam. In the present study, the relaxation rates of EO polymer optical waveguides were monitored in Mach–Zehnder interferometers (MZIs) by periodically measuring the increase in the half-wave voltage. The half-wave voltage (V_π), defined in Eq. (1), is the applied voltage required to change the phase of the light in one arm of the MZI relative to the other arm by 180°. Voltage can be applied to one or both arms of the MZI to modulate the intensity of the light at the output. The V_π is inversely proportional to the EO coefficient:

$$V_\pi = \lambda d / \left(n^3 r_{33} L \Gamma\right) \tag{1}$$

where λ is the wavelength of light being modulated, d is the distance between electrodes, n is the effective index of refraction of the waveguide, L is the length of the optical waveguide subjected to electrode modulation, and Γ is the optical–electrical overlap integral ($\Gamma = 1$ for our sandwich-electrode geometry).

In this paper we provide details for the synthesis of new chromophoric polymers, processing of thin films, fabrication of waveguide modulators, oven-aging, as well as the data reduction, modeling and multi-year aging predictions at elevated temperatures.

2. Experimental section

2.1. Polymer characterization: equipment and techniques

Differential scanning calorimetry (DSC) was performed on a TA Instruments, Inc. Model Q100. The DSC T_g was taken as the midpoint of the step transition observed on the 2nd or 3rd heating scan at 10 °C/min. The gel permeation chromatography (GPC) equipment used to measure molecular weight and polydispersity (PD) of the polyimides was a Viscotek, Inc., model 302-050; the columns were calibrated relative to polystyrene standards; the solvent was tetrahydrofuran (THF); and the ultraviolet–visible (UV–vis) detector was set at 640 nm. Nuclear magnetic resonance (NMR) analyses were performed with Brüker 300 MHz and/or Brüker 400 MHz instruments. A Cary 5 spectrophotometer was used to obtain the UV–vis spectra of the materials.

2.2. Materials

Two types of second-generation chromophores were used in this study: an isophorone-based chromophore called CLD [1] and a thiophene-based chromophore called FTC [1,3]. The EO core materials used in this investigation are listed in Table 1.

Table 1
List of electro-optic core materials used in this study

Designation	Material type	Bare dye/wt%[a]	T_g/°C
CLD–A/APC	Guest–host	26	145 ± 5[b]
CLD–A/APEC	Guest–host	26	150 ± 5[b]
FTC–A/APC	Guest–host	26	145 ± 5[b]
FTC–A/APEC	Guest–host	26	150 ± 5[b]
CLD–PI	Covalently attached	22	174 ± 3[c]
FTC–PI	Covalently attached	26	171 ± 3[c]

[a] For comparison with the side-chain attached materials, the weight percent of dye was calculated using just the bare-dye content (FTC–OH and CLD–OH containing only the *N*,*N*-(ethylhydroxyethyl) groups on the amine), based on molecular weights of 483 g/mol for FTC–OH, and 521 g/mol for CLD–OH. With the adamantane group attached, the CLD–A and FTC–A loadings were 34 wt%. Structures of the side-chain materials and chromophores are shown in Fig. 1 and discussed in Section 2.2.1.

[b] DSC measurements on pieces of ~100-μm thick films after multi-day baking at elevated temperature; midpoint of the transition at 10 °C/min.

[c] DSC measurements on powder-form dried materials; midpoint of the transition at 10 °C/min.

2.2.1. Guest chromophores

The guest chromophores, called FTC–A and CLD–A, were synthesized in our laboratory in batch sizes up to 80 g. "A" stands for the adamantane group attached to the chromophores. The adamantane group improved the pot life of the chromophores in spin-casting solutions and improved the solubility of the chromophores in the amorphous polycarbonate host materials. The bare chromophores, which contained only the *N*,*N*-(ethylhydroxyethyl)-amine group, were prepared by the method described in Ref. [9] for CLD–OH and by the improved method described in Ref. [10] for FTC–OH (the older method was described in Ref. [11]). Adamantane was attached to the penultimate precursors of FTC–OH and CLD–OH by reaction of the acid chloride of 1-adamantane carboxylic acid with the hydroxyethyl group of the dyes in the presence of 2 equiv of 4-dimethylaminopyridine (DMAP) at ambient. The most intense peaks of the electronic absorption spectra of FTC–A and CLD–A ranged from about 600 to 670 nm depending on the particular solvent used for the measurement.

2.2.2. Host polycarbonates

The amorphous polycarbonates used in this study were poly[bisphenol A carbonate-*co*-4,4′-(3,3,5-trimethylcyclohexylidene)diphenol carbonate]. APC (from Aldrich, catalog # 43,057-9) had a glass transition temperature (T_g) of 207 °C and APEC (Bayer AG, grade 9389 [12]) had a T_g of 215 °C. Both materials were obtained in pelletized form and used as-received.

2.2.3. Side-chain polyimides

The side-chain polymers were prepared in our laboratory. The structures of the FTC and CLD covalently attached to the polyimide backbones are shown in Fig. 1a and b. They

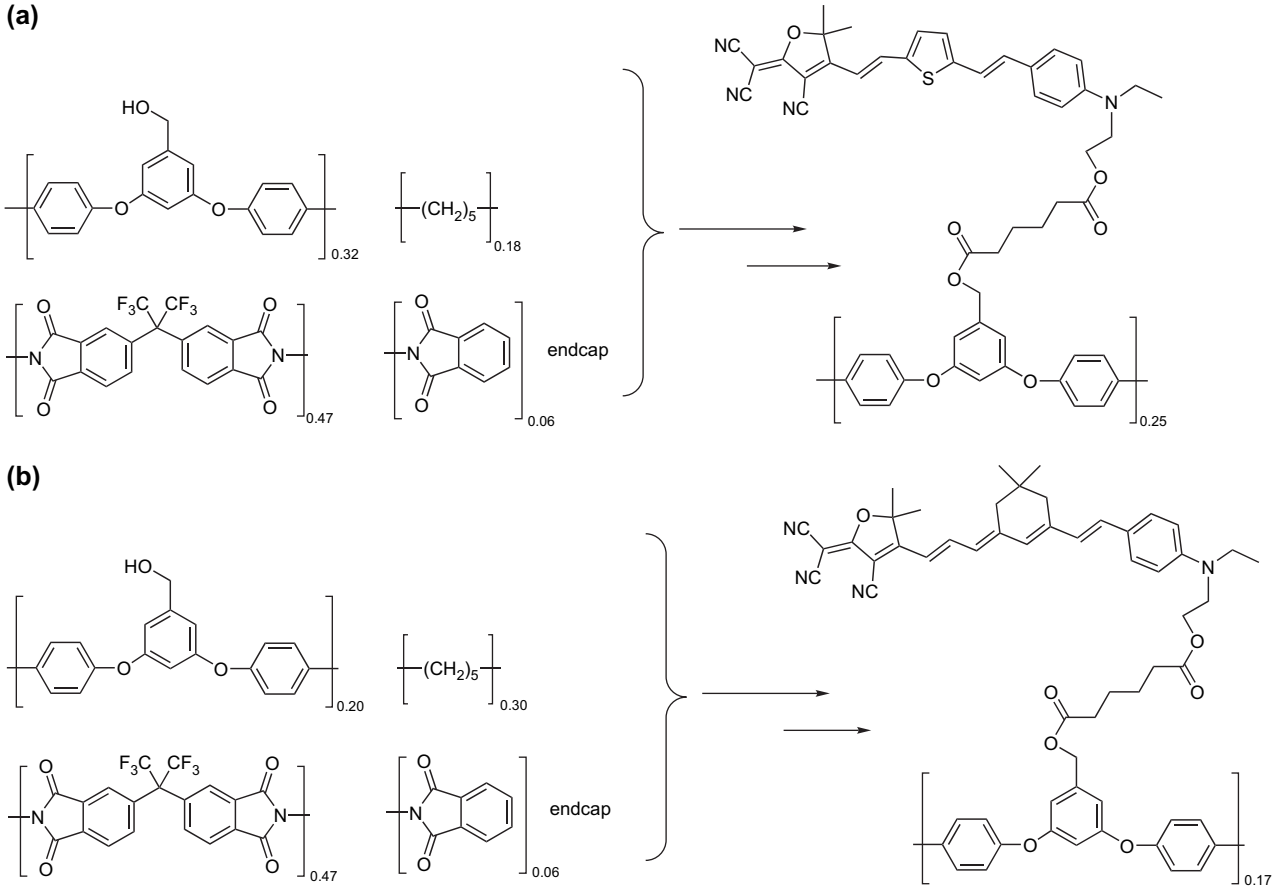

Fig. 1. (a) Polyimide backbone units and mode of FTC attachment (mole fractions are indicated); (b) polyimide backbone units and mode of CLD attachment (mole fractions are indicated).

were prepared via the method described in Ref. [13] with additional synthetic details provided below. All materials were designed to be compatible with the EO waveguide fabrication process [5,14,15].

The T_g was designed to be about 5 °C below the highest temperature at which CLD can be safely processed (~180 °C); FTC can be safely processed to ~210 °C. The T_g was tuned by adjusting the type and percentage of the flexible diamino monomer; we had a favorable experience with cadaverine. Consistent with our previous experience in attaching dyes to this type of polyimide [13,16], 78 mol% of the reactive sites (by proton NMR) on the starting polyimide became attached to the FTC dye and 85 mol% became attached to the CLD dye. UV–vis and GPC analyses supported this percentage of dye attachment [16].

The polyimide (PI) structures shown in Fig. 1 were designed to have a rather low molecular weight ($M_w = 5000$–7000 g/mol). This design eliminated gel formation in the case of CLD attachment reactions, which had been observed when using PI having a higher molecular weight. Gel was not seen when attaching other dyes to high molecular weight PI. Flexible spacer groups containing 4, 6, and 10 carbon atoms were investigated. The succinoyl ester (4 carbons) gave low dye attachment efficiency. The caproyl ester (10 carbons) gave polyimides that showed signs of phase separation. The adipoyl ester (6 carbons) was chosen for this study because it resulted in no phase separations, an adequate balance of properties, and relatively high attachment efficiency. The attachment chemistry is detailed below.

2.3. The preparation of the side-chain FTC–PI

Cadaverine (1,5-diaminopentane), adipoyl chloride, dichloromethane (anhydrous, non-stabilized), 5-*N*-methyl-2-pyrrolidinone (NMP, anhydrous grade), 4-dimethylaminopyridine (DMAP), tetrahydrofuran (THF) and phthalic anhydride were purchased from Aldrich (used as-received). 6FDA (2,2′-bis-(3,4-dicarboxyphenyl) hexafluoropropane dianhydride) was purchased from ChrisKev (Leawood, KS 66211) and used as-received. Synthesis of the diamino monomer containing the hydroxy benzyl side-attachment site, called BHB, has been published elsewhere [13]; the chemical structure is shown in Fig. 1.

2.3.1. FTC–PI step 1: preparation of the 32 mol% BHB–polyimide (shown in Fig. 1a)

A flask was charged with BHB (6.97 g, 21.0 mmol), cadaverine (1.207 g, 11.81 mmol), and NMP (60 mL). In one portion 6FDA (13.70 g, 30.84 mmol) and phthalic anhydride (583 mg, 6 mol% end-cap) were added to the solution that

was being rapidly stirred. An additional 20 mL of NMP was added to wash down the sides of the flask and the mixture was allowed to stir at ambient temperature for an additional 10 h. The flask was equipped with a reflux condenser and heated at 180 °C for 6 h. Then it was removed from the heating bath and allowed to cool for ~1 h. Then it was poured into a rapidly stirred methanol (1.5 L) solution. The precipitated polymer was stirred for ~1 h, collected on a glass frit, washed with methanol (~1 L) and then with ether (~300 mL). It was dried under reduced pressure (~0.2 torr) at 100 °C for 24 h to afford 19.2 g (90% yield) of light tan powder ($M_n = 5500$ g/mol, PD = 2.2; $T_g = 219$ °C), the 32% BHB–polyimide.

2.3.2. FTC–PI step 2: attaching the adipoyl side chain

A flask was charged with 4.00 g of the above BHB–polyimide, 2,6-di-*tert*-butyl-4-methylpyridine (800 mg), DMAP (80 mg), and THF (40 mL). Once all the materials had dissolved, adipoyl chloride (5.5 mL) was added in one portion and the mixture was allowed to react at ambient temperature for 16 h with stirring. This reaction slurry was filtered through a pad of Celite to remove the suspended salt, and the clear polymer solution passing through the Celite pad was added to ether (500 mL). The polymer precipitated in ether was collected on a frit and transferred directly into a 200 mL Schlenk flask for drying at 40 °C for ~1.3 h under reduced pressure.

2.3.3. FTC–PI step 3: attachment of the FTC–OH chromophore

The above modified polymer of 3.60 g was dissolved in 150 mL of dichloromethane; in one portion 2.00 g of the bare FTC–OH dye [10] was added to the mixture followed by an additional 30 mL of dichloromethane. The mixture was stirred for 10 min and then solid DMAP (prilled, 450 mg) was added in one portion; the mixture was allowed to react with stirring for an additional 3.5 h. The solution was concentrated to a volume of ~60 mL on a rotovap and the homogenous mixture was then poured into methanol (1.5 L). The polymer precipitated in methanol. It was collected and washed sequentially with methanol (500 mL), ether (300 mL), methanol (200 mL), and ether (100 mL); and then it was dried under reduced pressure to afford 5.10 g of a deep blue powder. After drying at 50 °C for 14 h under reduced pressure, NMR analysis of the sample indicated an attachment efficiency of about 78% and DSC indicated a final T_g of 171 °C. GPC analysis indicated that essentially all of the unattached FTC had been washed out of the polymer.

2.4. The preparation of the side-chain CLD–PI

The steps for preparing CLD–PI were very similar to those used in the FTC–PI preparation given above. However, an additional step was taken to remove residual (free) CLD–OH from the once-precipitated polymer. Approximately 2 g of dry, CLD–PI was redissolved in 20 mL of dichloromethane and precipitated a second time into methanol (500 mL). The solid was collected on a glass frit and washed with methanol (~200 mL) and then with ether (~300 mL). The polymer was dried at ~40 °C for 24 h at reduced pressure. By integration of the GPC chromatogram, it was determined that less than 4% of the total CLD in the sample was residual unattached CLD–OH. After this reprecipitation, analysis of the polymer by NMR spectroscopy indicated an attachment efficiency of about 85%. Analysis by DSC indicated that this material had a T_g of ~174 °C.

2.5. Films and modulator fabrication

The spin-casting solutions used to fabricate the waveguide core layers comprise 12% solids in 1,1,2,2-tetrachloroethane (the same solvent was used to prepare films of the guest–host and the side-chain polyimides) [16]. The guest–host solutions had about a 1-month pot life (even longer for the side-chain polyimides) when stored in an air-free environment in the dark.

A series of Mach–Zehnder interferometers (MZIs) were fabricated that contained polymer waveguides defined by a photobleaching method [5,14,15]. The MZIs contained micro-strip electrodes. Fig. 2 shows the geometry of the modulator and how light was coupled into and out of the waveguides.

The cross-section of the waveguide was a stack of electrode/cladding/core/cladding/electrode. The lower and upper claddings in all modulators were UV-cross-linked Norland 71® optical adhesive (Norland Products Inc., used as-received). The photobleaching extended through the entire thickness of the core layer leaving a high-index waveguide with a rectangular cross-section. The waveguide channel (EO material) was 3.5 μm thickness and 6 μm wide. To minimize UV-induced degradation of the chromophores, the upper cladding was cross-linked by a brief exposure to UV radiation followed by a 15-min thermal cure at 150 °C. The upper and lower cladding layers were of 3 μm thickness.

The entire poling cycle was carried out in a nitrogen-purged environment. To release trapped oxygen from the film during the poling cycle, samples were heated to about 100 °C and held at that temperature for 30 min. Next, a potential of 500 V was applied between the upper and the lower electrodes as the samples were heated to the highest temperature (145 °C for the guest–host materials and 170 °C for the side-chain polyimide materials). The dwell time at the highest temperature was about 2 min; then the samples were water-cooled to room temperature in about 20 min while maintaining the poling voltage [17]. A poling voltage of 500 V was found to give the best trade-off between high EO coefficient and low optical loss in the waveguides. The thermal history of all the

Fig. 2. A schematic of the polymer Mach–Zehnder modulator (top view) with free-space end-fire light coupling. The straight segments in the center (15-mm long, white lines) are the upper electrodes with connection pads; electrodes were not used in the Y-splitter and Y-coupler sections (also in shown in white).

modulators of this study was very similar throughout the initial heating, poling and cooling cycles.

The optical propagation loss (at 1550 nm wavelength) in the poled modulators was ~2.5 dB/cm for the GH materials and ~3.5 dB/cm for the SC materials (the higher value for SC materials could have been decreased, we believe, with more processing experience). We presumed that there was no phase separation in the GH materials, because that would have increased light scattering (optical loss) if the domain size of the phases was greater than 100 nm. The EO coefficient (for single-arm modulation) was ~35 pm/V for the FTC-based materials and ~39 pm/V for the CLD-based materials.

2.6. Modulator testing

The decrease of the electro-optic coefficient (r_{33}) was monitored by the increase in the V_π of the modulator. To make the V_π measurements, a light beam (1550 nm wavelength) was coupled into the waveguide of Mach–Zehnder interferometer using a microscope objective (as shown in Fig. 2). A low frequency (~DC) linear voltage ramp was applied to modulate the light in one of the arms. The V_π of the modulator was determined from the observed interference pattern. An initial measurement of V_π was made for each device at ambient. Modulators were placed in nitrogen-purged heated ovens for specified exposure times. A few modulators were stored at ambient temperature in air. Periodically, oven-aged modulators were cooled in nitrogen-purged storage containers to room temperature, after which V_π was measured in air (not more than 30-min air exposure per measurement). The optical power used for measuring V_π was less than 0.5 mW with a total light exposure time of about 10 min. During this multi-month oven-aging protocol, the temperature was cycled between the oven temperature and the room temperature one to two dozen times. Back-to-back measurements of V_π were repeatable to within ±0.1 V. Measurements made by different people on different days were repeatable to within ±0.3 V.

3. Results and discussion

Before heating Mach–Zehnder modulators to the oven-aging temperature, the average V_π was ~5.5 V for modulators based on CLD and ~6.5 V for those based on FTC (see Table 2). The lower V_π of CLD modulators may have been due to CLDs 15% larger molecular hyperpolarizability (as calculated via MOPAC® [18] taking into account the Z to E isomer ratio of our CLD, which was 26:74 by NMR [9]).

Table 2
Room-temperature aging data (aged in air)

EO core material	Initial V_π	Final V_π	Months between measurements
FTC–PI	6.3	6.8	12
CLD–PI-1	6.2	5.7	13
CLD–PI-2	5.7	5.6	12
CLD–PI-3	5.0	5.3	12

Table 2 shows 1-year room-temperature aging data (aged in air, in the dark) for modulators containing the side-chain polyimide core materials. All changes in V_π during ambient aging were within the experimental error of making an individual measurement. For guest–host materials (not shown) only 3 months of room-temperature aging were available, but the conclusion was the same (no change within experimental error).

3.1. Comparison of side-chain and guest–host materials

Three duplicate modulators were aged at 80 °C, and very good reproducibility of increase in V_π with time was observed (data not shown). Fig. 3 compares oven-aging data for modulators containing the side-chain (SC) and the guest–host (GH) core materials at 80 and 95 °C. Modulators containing SC materials had a much slower relaxation rate than did modulators containing the GH materials, which can be attributed not only to the higher T_g of the SC materials, but also to the tethering of the dyes (restricting mobility).

When the oven-aging temperature was increased from 80 to 95 °C, the change in V_π was much smaller for SC modulators than for the GH modulators. With the dye attached (SC polymers), there can be no sublimation of the dye at elevated temperatures. From UV–vis measurements of the GH films, less than 1% of the dye was lost due to sublimation while holding the sample for several hours at 150 °C. Although that type of measurement was not made during the months of aging in this study, we do not believe that a significant amount of dye was lost due to sublimation.

3.2. Comparison of CLD to FTC in the SC polyimide materials

The aging data for the FTC–PI and CLD–PI modulators are presented in Fig. 4. At 80 and 95 °C the relaxation rate

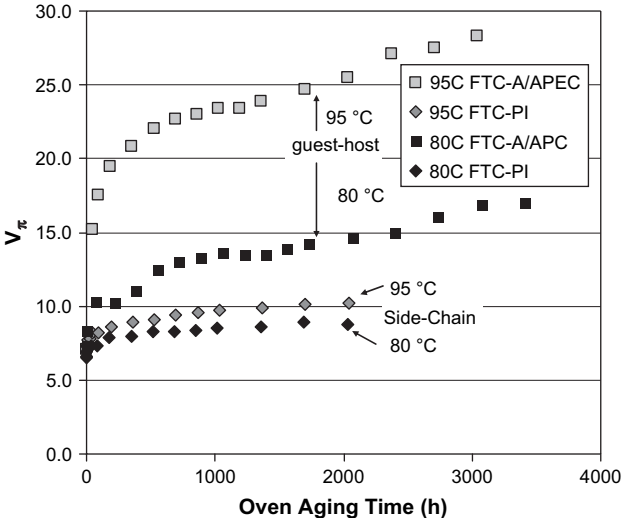

Fig. 3. Comparison of the covalently attached side-chain polyimide ($T_g = 171$ °C) and the guest–host polycarbonates ($T_g = 145$–150 °C), both types based on the FTC chromophore.

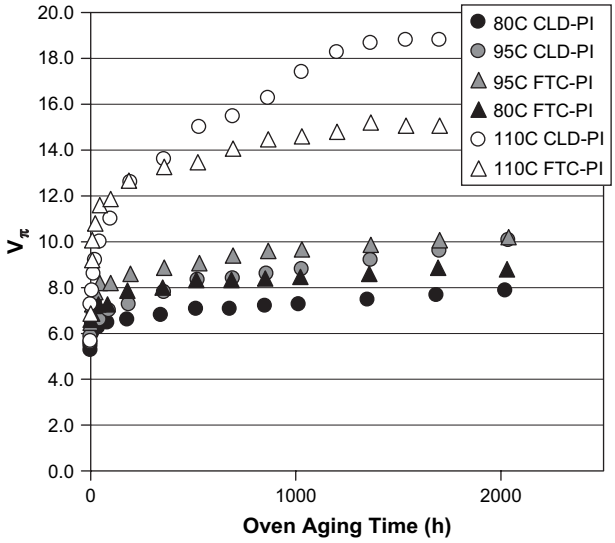

Fig. 4. A comparison of CLD and FTC side-chain polyimide core materials.

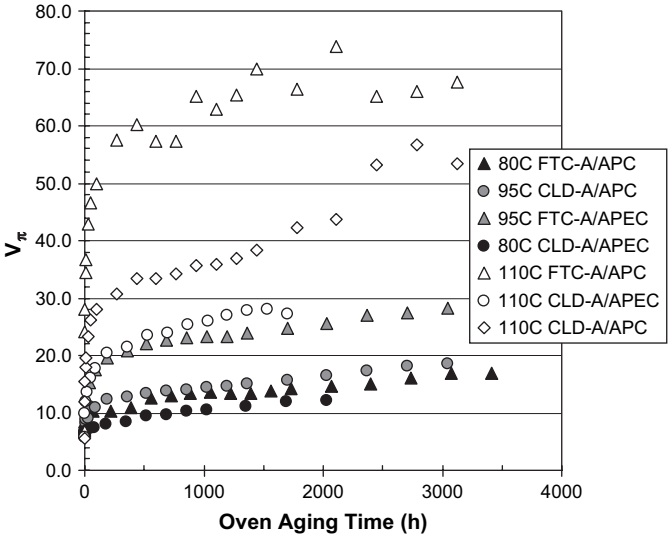

Fig. 5. A comparison of CLD–A and FTC–A in polycarbonate host materials.

was similar for both chromophores, and the V_π of the CLD–PI modulator remained lower than that of the FTC–PI modulator during the 2000-h test period. However, at 110 °C the aging curve of the CLD modulator crossed over and was higher than the curve of the FTC modulator (increasing faster than the FTC curve after the first 50 h of oven-aging).

The data at 110 °C were surprising, because CLD is a larger molecule than FTC and should, therefore, have a slower rotational diffusion rate. Furthermore, both polyimide materials have nearly the same glass transition temperature (171 vs. 174 °C, giving CLD–PI the slight edge again). Others have demonstrated that compared to FTC, CLD is more susceptible to photo-oxidative degradation [19]. We also have observed some optical loss in CLD modulators when exposed to air while guiding 1 mW of optical power at 1300 nm, but we saw no decrease in light intensity with FTC modulators under the same conditions. Relying on the protection of a nitrogen atmosphere in the oven, we did not add antioxidant to the films used in our modulators. It is possible that air diffused into the films during the roughly 30-min V_π measurements and did not have time to completely diffuse out of the films before reaching high temperatures in the nitrogen-purged oven. Therefore, we believe that the surprising increase in V_π at 110 °C for the CLD-based modulator is likely due to photo-oxidative degradation during the V_π measurements and/or oxidative degradation of CLD during aging at 110 °C. Duplicate modulators were not available to double-check these results.

3.3. Comparison of CLD–A to FTC–A in the polycarbonate GH materials

The GH aging data are shown in Fig. 5. The aforementioned unusual increase in V_π at 110 °C for the CLD modulator was not observed in CLD–A/polycarbonate until after 3 months of aging (the open diamonds). The polycarbonates were of injection-molding grades (used as-received). These grades normally contain antioxidants and light stabilizers that would have protected the CLD for an extended length of time. The cause of scatter in the 110 °C data (waviness) for the GH modulators is unknown, but the variation of V_π, when measured repeatedly within several minutes, was less than 1 V; therefore, the high voltage measurement by itself did not appear to change the material.

At 110 °C, it is clear that CLD–A out-performed FTC–A in APC. This may be attributed to the larger size of the CLD–A chromophore; its sweep area is ~20 to 25% larger than that of FTC–A [18] which would result in slower rotational diffusion. However, at a higher dye concentration not used in this study (35 wt% FTC–A and in APEC), we found that pieces of thick film that had been pre-baked for many days to remove solvent showed two glass transition temperatures by DSC (one near 90 °C) on each of four heating scans. Therefore, another hypothesis for the poor performance of the GH FTC–A modulator data shown in Fig. 5 (that film contained 34 wt% FTC–A) is that phase separation occurred and the T_g of the dye-rich phase was close to 110 °C.

CLD–A in APEC had a slower relaxation rate than it did in APC, which was not unexpected because the T_g of APEC is about 10 °C higher than the T_g of APC.

3.4. Seventeen months of aging

One of our modulators was aged for 17 months at 80 °C (perhaps the longest aging period at such a high temperature ever reported for an EO polymer). However, the poling conditions were different from that of the other modulators; therefore, it was not used in the modeling exercise below. In addition to showing the nearly 1.5 years of continuous aging at 80 °C, the data shown in Fig. 6 point out that the longer poling time may be responsible for a slightly lower V_π (due to physical aging). For the modulator poled for only 2 min (see Fig. 5), the curve for CLD–A/APEC at 80 °C shows that V_π was 12.5 V after 2000 h (and two other identical modulators, not shown, aged at 80 °C had V_πs of 12.6 and 13.3 V after

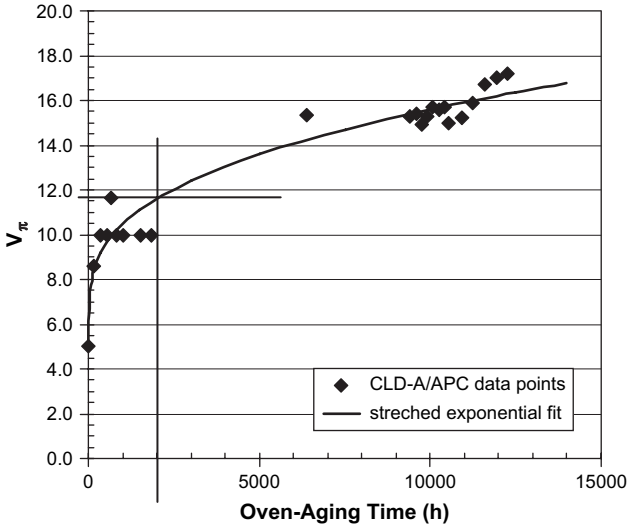

Fig. 6. Data for a 20-min poled CLD–A/APC modulator aged at 80 °C for 17 months.

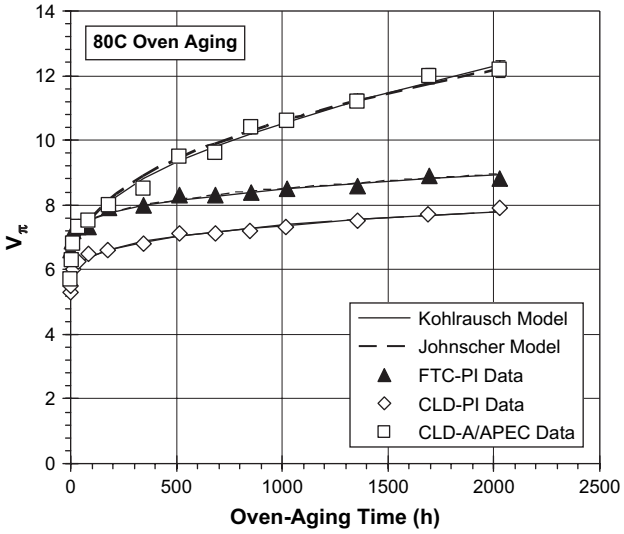

Fig. 7. Plots of the 80 °C oven-aging data for three types of EO polymers. The curves are least-squares fits for each equation (parameters for the functions are given in Table 3).

2000 h). For the CLD–A/APC modulator poled for 20 min (see Fig. 6), the V_π was 11.5 V after 2000 h at 80 °C (note that the host was APC, which should have given a higher V_π due to its lower T_g).

3.5. Isothermal aging models

For a quantitative description of our aging data we compared two nonlinear relaxation equations. These were written in terms of the increase in V_π (which is proportional to the decrease in r_{33}) vs. time. The well-known stretched exponential, proposed by Kohlrausch in 1847 [20], often called the KWW equation (for Kohlrausch–Williams–Watts [21] and references therein) has been used with much success by many investigators to fit nonlinear relaxation data of glassy EO polymers [7]. In terms of V_π, the reciprocal of r_{33}, we used Eq. (2) and call it Kohlrausch equation:

$$V_\pi(t)/V_\pi(0) = \exp\,(t/\tau)^b \tag{2}$$

where τ is a characteristic relaxation time constant of the EO material, t is aging time, and b is a measure of the breadth of the distribution of relaxation time constants. Kohlrausch stretched exponential equation is the same as the empirical Weibull equation which has long been used to predict reliability and aging in mechanical and biological systems [22].

Much of the polymer relaxation literature involves dielectric spectroscopy. Dureiko et al. reviewed aging models [23] and adapted a ''many-body'' approach [24] to successfully model the relaxation of poled polymers in both time and frequency domains. Closely related to this was Jonscher's earlier work [25], which showed that a broad range of unrelated materials have the same type of time–domain response to a step-function excitation. Jonscher's empirical law in the time domain has two power-law asymptotes: $[(t\omega_p)^{1+m} + (t\omega_p)^n]^{-1}$, where the peak of the dielectric loss (in the frequency spectrum) occurs at ω_p (the reciprocal of the characteristic time constant, τ). To model our sub-T_g oven-aging data, we used the following power law in time function, Eq. (3), which we call Jonscher equation:

$$V_\pi(t)/V_\pi(0) = 1 + (t/\tau)^j \tag{3}$$

Jonscher mentioned that a form of this equation, used for other applications, has been called the Curie–von Schweidler law [25].

3.6. Fitting models to the aging data

For aging at 80 °C, typical plots with the actual data points are shown in Fig. 7. Similar multi-month plots were made for aging at 95 and 110 °C (not shown); the curves were calculated by a least-squares fit [26] for both Eqs. (2) and (3). The time-zero point on all the relaxation plots was made at ambient, and the next point was taken after heating in the constant-temperature oven for 1 or 2 h. Eliminating the first point did not change the results (the same time constants were retrieved). Both Eqs. (2) and (3) fit all of the data well within the error bars for each V_π reading (±0.3 V). For all three elevated temperatures, Table 3 gives the values for the time constants, exponents, and goodness of fit for the various types of EO materials.

At 110 °C the FTC–PI modulator had the slowest aging rate and out-performed all other modulator materials in the long run. As expected from Fig. 5, FTC–A/APC at 110 °C had extremely small time constants; therefore, this material will not be given further consideration in this paper.

On the average, both Kohlrausch and Jonscher equations fit the several months of aging data equally well. However, when the sets of data were extrapolated to the out years, a large divergence between Jonscher and Kohlrausch equations was evident (the stretched exponential predicting a faster relaxation). Obviously, this has implications when trying to determine the

Table 3
Adjustable parameters sets for the EO materials

Temp./°C	Kohlrausch			Jonscher		
	τ_k (kh)	b	Chi sqr. [26]	τ_j (kh)	j	Chi sqr. [26]
FTC–PI						
80	193	0.263	1.3	75.7	0.289	1.2
95	101	0.202	2.6	22.2	0.234	2.8
110	8.37	0.138	2.5	0.57	0.18	2.5
CLD–PI						
80	119	0.233	4.2	36.3	0.262	6.6
95	12.6	0.31	5.6	4.33	0.360	6.0
110	0.66	0.217	3.5	0.115	0.321	2.8
CLD/APEC						
80	4.56	0.321	0.34	1.46	0.406	0.54
95	2.13	0.222	1.4	0.383	0.31	1.3
110	0.046	0.134	4.9	0.0047	0.236	2.9

practical lifetime of a device. Fig. 8 shows the 4-month oven-aging data for FTC–PI at 95 °C extrapolated to 20 years. The point of divergence is when aging time is longer than Jonscher time constant. As mentioned before, Refs. [23,25] say that Jonscher equation is consistent with causality, whereas there is some question in that regard for Kohlrausch equation. Therefore, we recommend giving Jonscher equation serious consideration for modeling relaxation of poled polymers.

3.7. Correlating the time constants with temperature: a brief summary of literature

After a glass-forming liquid is cooled from the melt and held at a constant temperature below the T_g, the density only slowly increases towards an equilibrium value (it is in a "super-cooled" state). Below T_g the chain segments and molecules are exceedingly crowded and jammed together so tightly that motion is greatly retarded. The glass may not come to an equilibrium density even after many years of aging. The continuing relaxation of the material is called physical aging.

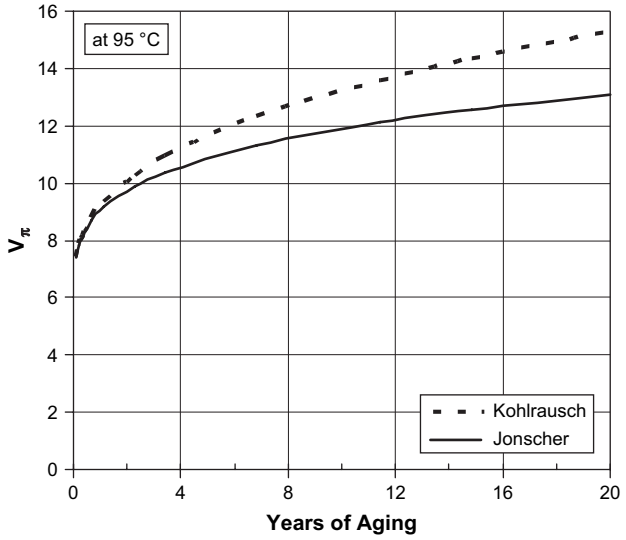

Fig. 8. Extrapolation to 20 years using 4-month oven-aging data for FTC–PI at 95 °C. Jonscher function predicts slower relaxation in the out years.

Even above the T_g, as the glass-forming liquid is cooled and approaches T_g, the material begins to deviate from Arrhenius behavior. This marks the onset of the transformation of liquid to glass that has been addressed by various phenomenological treatments by means of a characteristic reference temperature (an adjustable fitting parameter). These treatments have been relatively successful in predicting viscosity and related properties above and in the neighborhood of T_g. Two well-known, essentially identical treatments [7], are as follows: (1) $\ln(\tau) = -A + B/(T - T_o)$, Fulcher equation [27], which is also called the FTH treatment for Fulcher–Tammann–Hesse [28]; and (2) $\ln(\tau) = -C_1 + C_1C_2/(T - T_2)$, Williams–Landel–Ferry (WLF) equation [29].

In a glass, given a specific time–temperature history, a model for physical aging would ideally stipulate the degree of separation from equilibrium, and it would account for the molecular mechanisms and kinetics by which the material proceeds towards equilibrium. An equilibrium density (or enthalpy) of the glass at a given sub-T_g temperature can be estimated by extrapolating the actual property vs. temperature curve generated well above T_g. A modeling approach that makes use of this concept defines a reference temperature, which is called a fictive temperature. The fictive temperature, T_f, is the actual temperature at which the glass *would* be at equilibrium for the particular non-equilibrium state at which it presently finds itself. The fictive temperature changes with time. Hence, in the FTH and WLF relations, T_o and T_2 are not the fictive temperatures.

Tool was the first to define a fictive temperature [30]. Using Tool's groundwork, Narayanaswamy proposed a formal method to account for relaxation of glass-forming liquids and the memory effect [31]. Narayanaswamy contributed what is now called the TN description, which uses a reduced time integral to define a shift function that depends on T and T_f. Many improvements to the TN description have been proposed by others (see discussion and references in Ref. [32]). Hodge proposed improvements based on a distribution of activation energies [33,34], which has recently been called the Hodge–Scherer–Adam–Gibbs (HSAG) formula [35]. Prêtre et al. used many of the above fictive treatments to give a global temperature description of poled polymers at temperatures below, at, and above T_g [7], which enabled them to predict cooling rates and annealing times that would lower relaxation rates in poled EO polymers. It is beyond the scope of this paper to try to cover all of the studies on relaxation of poled polymers. However, a few more of the early references will be mentioned here. Ghabremichael et al. reviewed thermal and temporal stabilities in poled polymers including their own data and modeling [36]. Dhinojwala et al. studied the degree of coupling between the chromophore reorientation and the polymer α-relaxation process, and they developed a methodology for predicting thermal–temporal decay [37]. In addition to the WLF/FTH and fictive temperature treatments discussed above, many groups investigated different isothermal relaxation time distributions. The Hoechst Celanese Research group and ours considered a biexponential function [38,39]; the Max-Planck polymer group favored the symmetrical Havriliak–Negami

relaxation time distribution [40]; and the IBM-Almaden group investigated the log normal distribution of relaxation times [41]. There is some concern that one cannot assume a continuous distribution of relaxation times and neglect interactions between the relaxation modes (however, this concern may only be relevant where the deformation involved is not small).

Recently, Swallen et al. defined an "energy landscape" parameter, $\theta_k = (T_g - T_f)/(T_g - T_k)$ [42] where T_k is Kauzmann temperature [43], which is now generally defined as the temperature below which the configurational entropy is zero. Swallen et al. showed that the state of a glass can get "stuck" in a local energy minimum depending on how the material is processed and cooled. Their T_f was determined experimentally by integrating the DSC heat capacity vs. temperature and finding the intercepts of the glassy enthalpy curves with the liquid enthalpy curve extrapolated below T_g.

Royal and Torkelson found a characteristic sub-T_g temperature where the rate of physical aging was a maximum as measured by rotational diffusion rate of dyes [44]. The rotational diffusion rate of the poled chromophores is also greatly influenced by dipole–dipole interactions and chromophore size. We did not have enthalpy or density data for our materials above T_g (equilibrium data). Therefore, in this paper we have taken a phenomenological approach to model the effect of temperature. Since all of our samples underwent the same poling and quenching cycles, we assumed that the influence of physical aging was similar for all the modulators.

3.8. Fitting relaxation data as a function of temperature

Much of the early literature on relaxation of poled EO polymers involved materials containing the smaller, first-generation chromophores. Furthermore, most of those EO polymer modeling studies [36–40] used data from rather short aging periods near the glass transition temperature. Much of the early modeling work focused on free volume considerations. More recent studies give emphasis to local "potential energy landscapes" [35,42]. The scientific community has not yet arrived at a consensus on the best way to model relaxation in glass-forming liquids. Some authors believe that extrapolating a liquid's equilibrium properties to low temperatures is not well-founded [45]. There can be unpredictable differences in relaxation behaviors depending on how the chromophore is attached (or not) to the polymer. However, for a given type of EO polymer, and using a relatively constant thermal history in sample preparation, at this point in time, we feel a phenomenological approach with a manageable number of adjustable parameters is appropriate for extrapolating several months of data out to several years.

It has long been known that changes in characteristic relaxation time constants of glass-forming liquids follow simple Arrhenius behavior far below T_g and above T_g, but not in a transition zone in the neighborhood of T_g [25]. Therefore, our modeling approach incorporated that feature. At first, we attempted to correlate the data sets (time constants vs. temperature, taken from Eqs. (2) and (3)) using an activation-energy-based equation similar to a mirror image of Fulcher equation: $\ln(\tau/\tau_{ref}) = \{E_g - \Delta/[1 - (T/T_o)]\}/RT$ where τ_{ref} is a reference time constant (for liquid material), E_g is the thermal activation energy of rigid glassy material, $(1 - (T/T_o))^{-1}$ is a transition zone index, Δ is a thermal activation-energy parameter, and R is the ideal gas constant. Since this equation blows up at T_o and T_o was uncomfortably close to our upper aging temperature, although it gave a good fit to our sub-T_g data, this equation was abandoned.

For our next model (used for the rest of this study) we give the following morphological picture. Below T_g on a nanoscopic scale the bulk glass is a mosaic material consisting of rigid and pliable domains [34,45,46]. As the oven-aging temperature increases, the bulk glass undergoes thermal expansion, and in a "transition zone" (in the neighborhood of T_g) an increasingly large amount of rigid material converts into pliable material (shrinking the number and size of rigid domains). In addition to the chemical make-up of the material, the characteristics of the transition zone will also depend on the type of measurement being made, the time scale of the measurement, and thermal history (considered to be essentially constant in this study).

An attractive feature of our activation-energy-based equation (Eq. (4) shown below) is that it has no singularity point. The equation describes a smooth transition between the two Arrhenius-like temperature regions that lie on either side of the thermal transition zone (as measured by rotational diffusion of chromophores). The non-Arrhenius zone for our data extended quite far below the DSC T_g. The equation describing this model is as follows:

$$\ln(\tau/\tau_P) = E_R\left(1 + \tanh\left[\left(T_c - T\right)/D\right]\right)/2RT + E_p/RT \qquad (4)$$

where E_R and E_p are the thermal activation energies characteristic of rigid glassy molecular motion far below the transition zone and pliable molecular motion above T_g, respectively; tanh is the hyperbolic tangent; the $(1 + \tanh[(T_c - T)/D])/2$ term is a rigid-domain fill factor and defines the extent of the transition zone; R is the ideal gas constant; D is a delta temperature proportional to the breadth of the transition zone; and T_c is the central temperature of the transition zone [47]. Reasonable values for E_p are three orders of magnitude smaller than E_R (therefore, E_p is negligible below T_c). We found that by setting $\tau_P = 1$ s and neglecting E_p, Eq. (4) gave a good fit to our data. Increasing τ_P to 1 min gave a less satisfactory fit to the ambient relaxation data (discussed below).

The use of the hyperbolic tangent in a phenomenological model to transform the activation energy in the glass–rubber transition temperature zone has not been reported before (to our knowledge). We use it here to give emphasis to our conviction that the transformation mechanism in the region of T_g involves a spatially heterogeneous nanomorphology, and, in that regard, the tanh term represents a fill factor for the rigid molecular structure.

For each material, the parameter sets in Table 3 were used in each temperature-fitting process (one set from Jonscher equation and one set from Kohlrausch equation). The ambient

Table 4
Ambient parameter sets[a] for Eqs. (2) and (3)

Kohlrausch	*b*	τ (kh)
FTC–PI	0.51	12,300
CLD–PI	0.5	9300
CLD–A/APEC	0.69	160
Jonscher	*j*	τ (kh)
FTC–PI	0.50	3600
CLD–PI	0.6	2700
CLD–A/APEC	0.70	150[b]

[a] Values for exponents (*b* and *j*) were estimated by linear extrapolation (vs. temperature) of the three exponents obtained at higher temperatures. The time constants were estimated by extrapolating Eq. (4) to ambient (with the exception of APEC and Jonscher equation; see footnote (b).

[b] The extrapolated value from Eq. (4) was 36 kh; however, 150 kh is the minimum allowable ambient time constant by assuming V_π would increase not more than 0.3 V in 3 months [48].

parameters are given in Table 4 and discussed below. The time constants for the modulators are plotted in Figs. 9 and 10. Eq. (4) fit the FTC–PI data better than to the CLD–PI data. The unusual shape of the CLD–PI curve was probably caused by some degree of chemical degradation of the CLD chromophore (otherwise, we would have expected the 95 and 110 °C time constants to be as high as, or higher than, the FTC–PI time constants). A good fit was also obtained for the CLD–A/APEC parameter set from Kohlrausch equation (Table 5).

Regarding the estimation of ambient time constants, we found no change in V_π (±0.3 V) after months of aging (Table 2). Therefore, the ambient time constants could be close to infinity, but more likely they are closer to the values extrapolated to ambient using Eq. (4). We calculated what would be the smallest possible ambient time constants using Eqs. (2) and (3), plugging

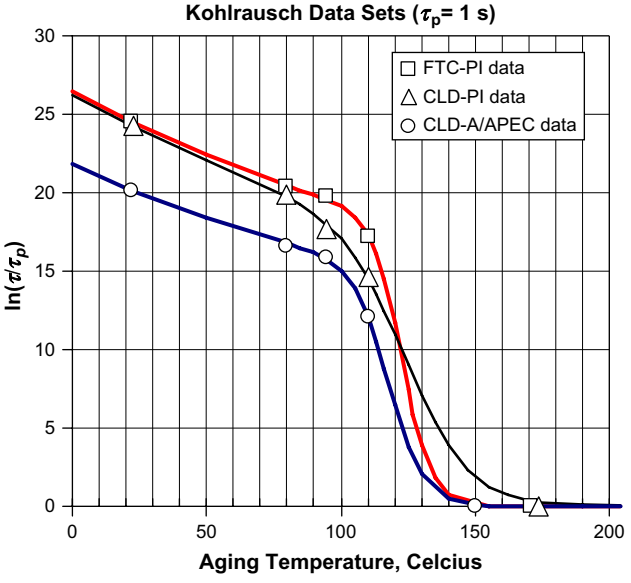

Fig. 9. The data points were generated by Kohlrausch equation using the high-temperature parameter sets in Table 3. The curves were generated by Eq. (4) using the parameter sets in Table 5. The room-temperature points were not included in the least-squares fitting process.

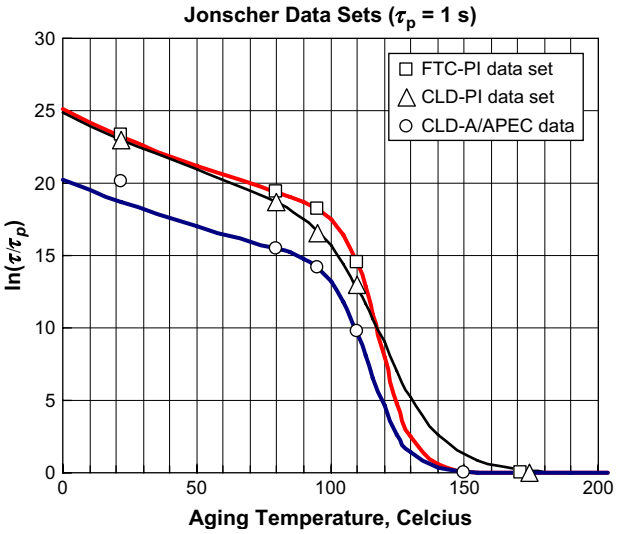

Fig. 10. The data points were generated by Jonscher equation using the high-temperature parameter sets in Table 3. The curves were generated by Eq. (4) using the parameter sets in Table 5. The room-temperature points were not included in the least-squares fitting process.

in $V_\pi = V_\pi(t) + 0.3$ where *t* was the actual aging period, and using exponents obtained by linearly extrapolating the high-temperature exponents for each material to ambient. For the side-chain polyimide modulators, this method gave time constants very close to those predicted by Eq. (4) for both Jonscher and Kohlrausch parameter sets. For the CLD guest–host modulators this was only true for Kohlrausch parameter set (see Table 4) [48].

Eq. (4) gave a good fit through the time constants obtained from both Jonscher and Kohlrausch equations at the three oven-aging temperatures. The small differences in the goodness of fit between Jonscher and Kohlrausch equations are to be expected for aging periods no longer than the time constants. For the guest–host Jonscher data set the ambient time constant predicted by Eq. (4) being lower than the data will allow is an unresolved discrepancy.

Table 5
Parameters sets used for Eq. (4) in correlating the time constants with the oven-aging temperatures[a]

Material	T_c/°C	*D*/K	(E_R/R)/K	Fit[b] $\sum(x-y)^2$
Kohlrausch, Eq. (2)				
FTC–PI	123	11	7230	0.05
CLD–PI	125	24	7150	0.21
CLDA/APEC	118	13	5950	0.05
Jonscher, Eq. (3)				
FTC–PI	119	12.5	6860	0.006
CLD–PI	121	23	6780	0.05
CLD–A/APEC	115	14	5510	0.006

[a] Only the three high-temperature data points were used in the fitting process. These parameter are based on $\tau_p = 1$ s.

[b] The Excel® sum-of-squares-of-differences: $\sum(x-y)^2$ where $x = \ln(\tau/\tau_P)$ calculated with Eq. (4) parameters, and $y = \ln(\tau'/\tau_P)$ where τ' values are from Eqs. (2) and (3) fit through the original V_π vs. time data. Differences of ± 0.05 in $\sum(x-y)^2$ were not considered significant.

3.9. Extrapolating the models to 10 years of aging

Eq. (4) can be used to interpolate and extrapolate V_π (or r_{33}) to any temperature by plugging its value of $\tau(T)$ into Eq. (2) or (3). The fitting parameters given in Tables 3 and 4 for Kohlrausch and Jonscher equations were used to estimate the V_π after 10 years of continuous aging at various temperatures. The calculated V_πs were normalized to the time-zero values (see Table 6).

For the polyimide modulators, at 80 °C these functions predict that the V_π would be slightly more than double in 10 years (r_{33} would drop to 50%). Jonscher function predicts the same or lower V_π than Kohlrausch function for all the materials at every temperature. The CLD modulator data at 110 °C were not reported, because oxidation and photodegradation likely caused inordinately high values.

We feel that the data for FTC–PI can fairly confidently be interpolated and extrapolated with our modeling equations. Many commercial specifications call for 85 °C as a standard aging temperature. Using the interpolated time constants from Eq. (4) and the interpolated exponents from Eqs. (2) and (3), the V_πs were calculated for 10 years of aging at 85 °C for the FTC–PI modulators. Starting at 6.3 V, the V_π values were 13 and 15 V, for Jonscher and Kohlrausch equations, respectively (normalized values are 2.1 and 2.4, respectively).

We considered what value Eq. (4) would predict for V_π if material properties were changed for the FTC–PI material (for example, by stiffening the backbone and/or shortening the tether). Using Jonscher function, if only E_R is increased, after oven-aging at 85 °C/10 years, a 50% increase in E_R greatly attenuates the increase in V_π (starting at 6.3 V it increases to only 6.9 V). If the T_g of the polymer is increased, likely both T_c and E_R would increase. However, if we increase only the T_c (e.g., by the same number of degrees that T_g increases), rotational diffusion would be significantly attenuated only at temperatures within the transition zone.

Presumably, the decrease of r_{33} in our modulators could have been significantly retarded by in-field annealing (physical aging) during the initial poling process. For example, others have shown that after poling a few minutes at T_g, the sample should be cooled and held isothermally ~30 °C below the DSC T_g for an hour while the poling voltage is maintained, and only then cooled to ambient [7,38,49,50].

Table 6
Estimated V_π after 10 years of oven-aging (normalized to $V_\pi(0) = 1$)[a]

	Ambient	80 °C	95 °C	110 °C
FTC–PI				
Kohlrausch	1.1	2.2	2.6	3.7
Jonscher	1.1	2.0	2.4	3.5
CLD–PI				
Kohlrausch	1.1	2.5	6.2	–
Jonscher	1.1	2.3	3.0	–
CLD–A/APEC				
Kohlrausch	1.9	13	9.8	–
Jonscher	1.7	6.3	6.3	–

[a] The parameter sets used to calculate the 10-year V_π values are given Tables 3 and 4.

4. Conclusions

For the side-chain polyimide (PI) materials (T_g ~ 170–175 °C), the electro-optic coefficient (r_{33}) decreased 30% after 3 months oven-aging at 80 °C, as determined from the increase in half-wave voltage (V_π) of Mach–Zehnder modulators. For the polycarbonate guest–host materials (T_g ~ 145–150 °C) at the same aging conditions, the r_{33} decreased 50%. The starting V_πs for the CLD- and FTC-based single-arm modulators were ~5.5 and 6.5 V, respectively. At the elevated aging temperatures, all modulators were kept in a nitrogen atmosphere, and occasionally tested with a light source operating at 1550 nm and at <0.5 mW. Therefore, we believe that the decrease in V_π at 80 °C was nearly completely due to rotational diffusion of the chromophores. After months of aging at 110 °C, we saw evidence of a slight amount of chemical degradation in the CLD materials; but not for the FTC materials. With that caveat, we believe conclusions can be drawn from our modeling study that will have practical application. In the data-fitting process for determining the relaxation time constants, the power law in time model predicted a significantly slower relaxation rate for long aging periods than the stretched exponential model (a ~ 10% difference after 10 years at 95 °C). A new activation-energy equation for correlating relaxation time constants with temperature was demonstrated. Our aging model, which was fit through the data and extrapolated, predicted that the V_π of the FTC–PI modulator would double after 10 years of aging at 85 °C. Continued development of an FTC side-chain polyimide having a T_g ~ 190 °C is recommended for the demonstration of low-cost, high-frequency, electro-optic devices. Also recommended for future study is: (1) the use of antioxidants and light stabilizer additives, (2) poling while annealing below the glass transition temperature (taking advantage of physical aging), and (3) cross-linking the material during poling to increase multi-year stability.

Acknowledgements

This work was supported by the Office of Naval Research (ONR), with additional support from DARPA for completing the modeling. The authors would like to acknowledge the following NAVAIR personnel: Michael Bramson for helpful discussions, Matthew Davis and Richard Hollins for chromophore synthesis, Stephen Fallis for help with BHB monomer synthesis; Dan Bliss for GPC and DSC measurements; Andy Chafin for MOPAC® calculations; and the following AMRDEC personnel: Charlotte Ingram and Mike Watson for poling, and Eric Webster for polymer processing.

References

[1] Shi Y, Zhang C, Zhang H, Bechtel JH, Dalton LR, Robinson BH, et al. Science 2000;288:119–22.

[2] Bortnik B, Hung YC, Tazawa H, Seo BJ, Luo J, Jen A, et al. IEEE J Sel Top Quant Electron 2007;13:104–10.
[3] Dalton LR, Steier WH, Robinson BH, Zhang C, Ren A, Garner S, et al. J Mater Chem 1999;9:1905–20.
[4] Robinson BH, Dalton LR, Harper AW, Ren A, Wang F, Zhang C, et al. Chem Phys 1999;245:35–50.
[5] Ashley PR, Temmen MG, Diffey WM, Sanghadasa M, Bramson MD, Lindsay GA, et al. Proc SPIE 2006;6314: 63140J-1-11.
[6] Mortazavi MA, Knoesen A, Kowel ST, Henry RA, Hoover JM, Lindsay GA. Appl Phys B 1991;53:287–95.
[7] Prêtre P, Meier U, Stalder U, Bosshard C, Günter P, Kaatz P, et al. Macromolecules 1998;31:1947–57.
[8] Park HP, Lee CH, Herman WN. Opt Express 2006;14:8866–84 and references therein.
[9] Davis MC, Chafin AP, Hollins RA, Baldwin LC, Erickson ED, Zarras P, et al. Synth Commun 2004;34:3419–29.
[10] Davis MC, Hollins RA, Douglas B. Synth Commun 2006;36:3515–23.
[11] Koeckelberghs G, Sioncke S, Verbiest T, Persoons A, Samyn C. Polymer 2003;44:3785–94.
[12] Dasgupta S. General Electric Global Research Center, provided the sample of APEC 9389.
[13] Wright ME, Fallis S, Guenthner AJ, Baldwin LC. Macromolecules 2005; 38:10014–21.
[14] Diffey WM, Trimm RH, Temmen MG, Ashley PR. J Lightwave Technol 2005;23:1787–90.
[15] Sanghadasa M, Ashley PR, Webster EL, Cocke C, Lindsay GA, Guenthner AJ. J Lightwave Technol 2006;24:3816–23.
[16] Guenthner AJ, Wright ME, Fallis S, Lindsay GA, Petteys BJ, Yandek GR, et al. Proc SPIE 2006;6331: 63310M-1-11.
[17] Watson MD, Ashley PR, Abushagur MAG. IEEE J Quantum Electron 2004;30:1555–61.
[18] Chafin AJ. Calculations performed at NAVAIR, China Lake, CA 93555, USA.
[19] DeRosa ME, He M, Cites JS, Garner SM, Tang YR. J Phys Chem B 2004;108:8725–30.
[20] Kohlrausch R. Ann Phys Chem (Leipzig) 1847;72:353–406.
[21] Chung SH, Stevens JR. Am J Phys 1991;59:1024–30.
[22] Weibull W. J Appl Mech Trans ASME 1951;18:293–7.
[23] Dureiko RD, Schuele DE, Singer KD. J Opt Soc Am B 1998;15:338–50.
[24] Dissado LA, Hill RM. Nature 1979;279:685–9.
[25] Jonscher AK. Nature 1977;267:673–9.
[26] Levenberg–Marquardt nonlinear least-square routine used on MATLAB®.
[27] Fulcher GS. J Am Ceram Soc 1925;8:339–55.
[28] Tammann Von G, Hesse W. Z Anorg Allg Chem 1926;156:245–57.
[29] Williams ML, Landell RF, Ferry JD. J Am Chem Soc 1955;77:3701–7.
[30] Tool AQ. J Am Ceram Soc 1946;29:240–53.
[31] Narayanaswamy OS. J Am Ceram Soc 1971;54:491–8.
[32] Chow TS, Prest Jr WM. J Appl Phys 1982;53:6568–73.
[33] Hodge IM. Macromolecules 1986;19:938–41.
[34] Hodge IM. Macromolecules 1987;20:2897–908.
[35] Lubchenko V, Wolynes PG. J Chem Phys 2005;121(7):2852–65.
[36] Ghabremichael F, Kuzyk MG, Lackritz HS. Prog Polym Sci 1997;22: 1147–201.
[37] Dhinojwala A, Hooker JC, Torkelson JM. In: Lindsay GA, Singer KD, editors. Polymers for second-order nonlinear optics. ACS symposium series 601. Washington, DC: American Chemical Society; 1995. p. 318–32.
[38] Man HT, Yoon HN. Adv Mater 1992;4(3):159–68.
[39] Lindsay GA, Henry RA, Hoover JM, Knoesen K, Mortazavi MA. Macromolecules 1992;25:4888–94.
[40] Winkelhahn HJ, Neher D, Servay TK, Rengel H, Pfaadt M, Böffel C, et al. In: Miyata S, Sasabe H, editors. Poled polymers and their applications to SHG and EO devices, advances in nonlinear optics, vol. 4. Gordon and Breach Science Publishers; 1997. p. 179–94.
[41] Verbiest T, Burland DM, Walsh CA. Macromolecules 1996;29:6310–6.
[42] Swallen SF, Kearns KL, Mapes MK, Kim YS, McMahon RJ, Ediger MD, et al. Science 2007;315:353–6.
[43] Kauzmann W. Chem Rev 1948;43:219–56.
[44] Royal JS, Torkelson JM. Macromolecules 1993;26:5331–5.
[45] Thurau CT, Ediger MD. J Chem Phys 2003;118:1996–2004.
[46] An amorphous glass has molecular packing defects or it would be a crystal. On a molecular scale, a segment near a defect (a nano-void) is "pliable," because when given a thermal nudge, it has a greater probability of changing its conformation than a segment not near a defect (a "rigid" segment). As the sample is heated, pliable regions would grow in size at the expense of surrounding rigid material. In the hypothetical model, at a given temperature the pliable (more mobile) domains would have a characteristic (mean) size, and there would be a distribution of pliable domain sizes. Surface tension would likely play a role in the formation of this mosaic morphology [35]. The pliable regions may be somewhat interpenetrating throughout the bulk material. Pliable domains would be closer to a state of equilibrium than the rigid domains, and perhaps at some sub-T_g temperature the larger pliable domains would be in a state of equilibrium.
[47] The characteristic temperature of the model (T_c) would be reached when the mean size of the distribution of pliable domain (or mobile domain) sizes is the same size as the chromophore. In the case of very small chromophores (aminonitrobenzene, as an extreme example), T_c would occur at a lower temperature than that for the larger chromophores of this study.
[48] Ambient aging measurements were available for the closely related CLD–N/APEC modulators (N stands for the norbornene group), for which there were no changes in V_π ($\pm$0.3 V) in 3 months at ambient. Measurements were not available for the CLD–A/APEC guest–host material; however, we assumed that CLD–A/APEC modulators would exhibit the same aging behavior, i.e., not more than 0.3 V increase in 3 months.
[49] Shen Q, Wong KY. Opt Commun 1999;164:47–50.
[50] Hampsch HL, Yang J, Wong GK, Torkelson JM. Polym Commun 1988; 30:40–3.